Mutations in *VPS13D* Lead to a New Recessive Ataxia with Spasticity and Mitochondrial Defects

Eunju Seong, PhD,[1] Ryan Insolera, PhD,[2] Marija Dulovic, PhD,[3] Erik-Jan Kamsteeg, PhD,[4] Joanne Trinh, PhD,[3] Norbert Brüggemann, MD,[5] Erin Sandford, PhD,[1] Sheng Li, PhD,[1] Ayse Bilge Ozel, PhD,[6] Jun Z. Li, PhD,[6,7] Tamison Jewett, MD,[8] Anneke J. A. Kievit, MD, PhD,[9] Alexander Münchau, MD,[3] Vikram Shakkottai, MD, PhD,[10] Christine Klein, MD,[3] Catherine A. Collins, PhD,[2] Katja Lohmann, PhD,[3] Bart P. van de Warrenburg, MD, PhD,[11] and Margit Burmeister, PhD[1,6,7,12]

Objective: To identify novel causes of recessive ataxias, including spinocerebellar ataxia with saccadic intrusions, spastic ataxias, and spastic paraplegia.
Methods: In an international collaboration, we independently performed exome sequencing in 7 families with recessive ataxia and/or spastic paraplegia. To evaluate the role of *VPS13D* mutations, we evaluated a *Drosophila* knockout model and investigated mitochondrial function in patient-derived fibroblast cultures.
Results: Exome sequencing identified compound heterozygous mutations in *VPS13D* on chromosome 1p36 in all 7 families. This included a large family with 5 affected siblings with spinocerebellar ataxia with saccadic intrusions (*SCASI*), or spinocerebellar ataxia, recessive, type 4 (*SCAR4*). Linkage to chromosome 1p36 was found in this family with a logarithm of odds score of 3.1. The phenotypic spectrum in our 12 patients was broad. Although most presented with ataxia, additional or predominant spasticity was present in 5 patients. Disease onset ranged from infancy to 39 years, and symptoms were slowly progressive and included loss of independent ambulation in 5. All but 2 patients carried a loss-of-function (nonsense or splice site) mutation on one and a missense mutation on the other allele. Knockdown or removal of *Vps13D* in *Drosophila* neurons led to changes in mitochondrial morphology and impairment in mitochondrial distribution along axons. Patient fibroblasts showed altered morphology and functionality including reduced energy production.
Interpretation: Our study demonstrates that compound heterozygous mutations in *VPS13D* cause movement disorders along the ataxia–spasticity spectrum, making *VPS13D* the fourth VPS13 paralog involved in neurological disorders.

ANN NEUROL 2018;00:000–000

View this article online at wileyonlinelibrary.com. DOI: 10.1002/ana.25220

Received Nov 1, 2017, and in revised form Mar 11, 2018. Accepted for publication Mar 19, 2018.

Address correspondence to Dr Burmeister, Molecular and Behavioral Neuroscience Institute, University of Michigan, 5061 BSRB, 109 Zina Pitcher Place, Ann Arbor, MI 48109-2200, E-mail: margit@umich.edu; Dr van de Warrenburg, Department of Neurology 935, Donders Institute for Brain, Cognition, and Behavior, Radboud University Medical Centre, PO Box 9101, 6500 HB, Nijmegen, the Netherlands, E-mail: Bart.vandeWarrenburg@radboudumc.nl; and Dr Lohmann, Institute of Neurogenetics, University of Lübeck, Maria-Goeppert-Straße 1, 23562 Lübeck, Germany; E-mail: katja.lohmann@neuro.uni-luebeck.de

From the [1]Molecular and Behavioral Neuroscience Institute, University of Michigan, Ann Arbor, MI; [2]Department of Molecular, Cellular, and Developmental Biology, University of Michigan, Ann Arbor, MI; [3]Institute of Neurogenetics, University of Lübeck, Lübeck, Germany; [4]Department of Human Genetics, Radboud University Medical Centre, Nijmegen, the Netherlands; [5]Department of Neurology, University of Lübeck, Lübeck, Germany; [6]Department of Human Genetics, University of Michigan, Ann Arbor, MI; [7]Department of Computational Medicine and Bioinformatics, University of Michigan, Ann Arbor, MI; [8]Department of Pediatrics, Section on Medical Genetics, Wake Forest School of Medicine, Winston-Salem, NC; [9]Department of Clinical Genetics, Erasmus MC, Rotterdam, the Netherlands; [10]Departments of Neurology and Molecular and Integrative Physiology, University of Michigan, Ann Arbor, MI; [11]Department of Neurology, Donders Institute for Brain, Cognition, and Behavior, Radboud University Medical Centre, Nijmegen, the Netherlands; and [12]Department of Psychiatry, University of Michigan, Ann Arbor, MI

Current address for Sheng Li: Bio-X Center, Shanghai Jiao Tong University, China

Ataxia is a symptom of >400 syndromic neurological conditions or can be the sole symptom of >80 recessively, dominantly, or X-linked inherited genetically defined conditions.[1–3] Recessive forms of ataxia are clinically and genetically more heterogeneous than dominant ataxias. Only in a minor fraction (~20%) of idiopathic or suspected recessive ataxia cases can a mutation in a known ataxia gene be identified,[4] suggesting that much of the genetic heterogeneity still remains to be discovered. In addition to heterogeneity, there is also pleiotropy, as the spectrum of ataxias also includes clinical and molecular overlap with, for example, the spastic paraplegias.[5]

Here, we report 12 patients from 7 families with compound heterozygous mutations in *VPS13D*. All patients > 2 years old have ataxia and/or spasticity, whereas the one 2-year-old patient shows developmental delay and hypotonia and is nonambulatory (see Supplementary Table). The phenotype in 1 of these families, comprising 5 patients (Fig 1), has previously been described in detail.[6,7] Briefly, patients in this family demonstrated early adult onset cerebellar ataxia with neuropathy and pyramidal signs, as well as striking saccadic intrusions, hence initially referred to as spinocerebellar ataxia with saccadic intrusion (*SCASI)*,[6] later renamed spinocerebellar ataxia, recessive, type 4 (*SCAR4)*. Analysis of *Drosophila* knockout models and patient-derived fibroblasts suggests that mutations in this new ataxia/spasticity gene impact on mitochondrial structure and function.

Materials and Methods

Patients

Patients were identified in 5 different centers with a focus on movement disorders located at Case Western Reserve University (Cleveland, OH) and genetically analyzed in Ann Arbor (MI, UM1), Nijmegen and Rotterdam (the Netherlands, NIJ1–4), Lübeck (Germany, LUB1), and Winston-Salem (NC, USA, WF1). Diagnostic testing (including gene panel analysis of known ataxia/spasticity genes) did not reveal a molecular diagnosis in these cases. All patients and relatives gave written informed consent to participate in diagnostic or research studies that were approved by the respective local institutional review boards (Institutional Review Boards of the University of Michigan Medical School, University of Lübeck ethics review panel), or to local (NIJ and Rotterdam) or commercial (WF1; GeneDx, Gaithersburg, MD) clinical exome sequencing (NIJ and WF1). Formation of this collaboration was facilitated by publication of grants funded by the National Ataxia Foundation and by GeneMatcher.[8]

Genetic Studies: Linkage Analysis and Exome Sequencing

In Family UM1, linkage analysis was performed with DNA from all 5 affected members, the mother, and 7 unaffected siblings using the Infinium HumanLinkage-24 Beadchip kit (6,000 markers, WG-32-140; Illumina, San Diego, CA), followed by parametric fully penetrant recessive model analysis in Merlin.[9]

In all families, whole exome sequencing was performed by exome capture (UM1: SeqCap EZ Exome Kit v3.0 [Roche Sequencing, Pleasanton, CA] at UM core facility; LUB1: NexteraRapid Exome Capture Kit [Illumina] at Centogene [Rostock, Germany]; all NIJ cases and WF1: SureSelectXT Human All Exon 50Mb Kit V5 [Agilent Technologies, Santa Clara, CA] at BGI Copenhagen [NIJ] and at GeneDx [WF1]) followed by next generation sequencing on Illumina arrays (UM1 and LUB1: paired end HiSeq2000; LUB1: NextSeq500) to medium coverage of 46× (UM1) or to ~75× (all NIJ, LUB1, and WF1).

For UM1, 2 cases were sequenced and variant analysis was restricted to the ~10Mb linkage region. For LUB1, WF1, and NIJ4, parents were also sequenced and initially, a trio analysis for de novo variants (no damaging hits) was performed. Variants were called as follows. For UM1.1 and UM1.4, alignment was done using Burrows-Wheeler Aligner against Human 1K Genome reference, duplicates were removed using Picard (v1.74), base recalibration, realignment, and variant calling were done using GATK (v3.3); these samples were part of a 734-sample pooled call. For LUB1, variant calling was performed as described.[10] For NIJ, clinical exome sequencing and variant calling were performed as described.[11] For WF1, GeneDx clinical whole exome pipeline was employed. Detected variants were filtered for rare (European population frequency < 0.01) and protein-changing variants under a recessive model. *VPS13D* variants emerged as the strongest candidate in all cases.

All *VPS13D* variants were Sanger confirmed and segregation in the family consistent with compound heterozygosity was verified.

Copy number variant analysis was not performed on all samples. Because single exonic deletions are difficult to detect in whole exome analyses, they cannot be ruled out. Because all patients were compound heterozygous, a whole gene deletion in *VPS13D* can be ruled out.

Analysis of Expression: Nonsense-Mediated Decay and Splice Site Prediction

Because *VPS13D* expression is higher in skin (fibroblasts) than in blood, we used mRNA extracted from a fibroblast culture to study expression levels and nonsense-mediated mRNA decay (NMD) in Family UM1 (data not shown) and Patient LUB1.1. For Patient LUB1.1, RNA was extracted using the QIAmp RNA Extraction Kit (Qiagen, Germantown, MD). Oligo-dT-nucleotides of the Maxima First Strand cDNA Synthesis Kit (Thermo Fisher Scientific, Waltham, MA) served as primers to synthesize the complementary DNA (cDNA) by use of reverse transcriptase (RT). Polymerase chain reaction (PCR) was performed with primers in exons 21 and 22 (VPS13Dex21F: TGATTCCTTAGTCCA CATCAAC; VPS13Dex22R: ATCATTTCCAGGTGTGC TAC), and the respective product was inspected for its size and Sanger sequenced. Furthermore,

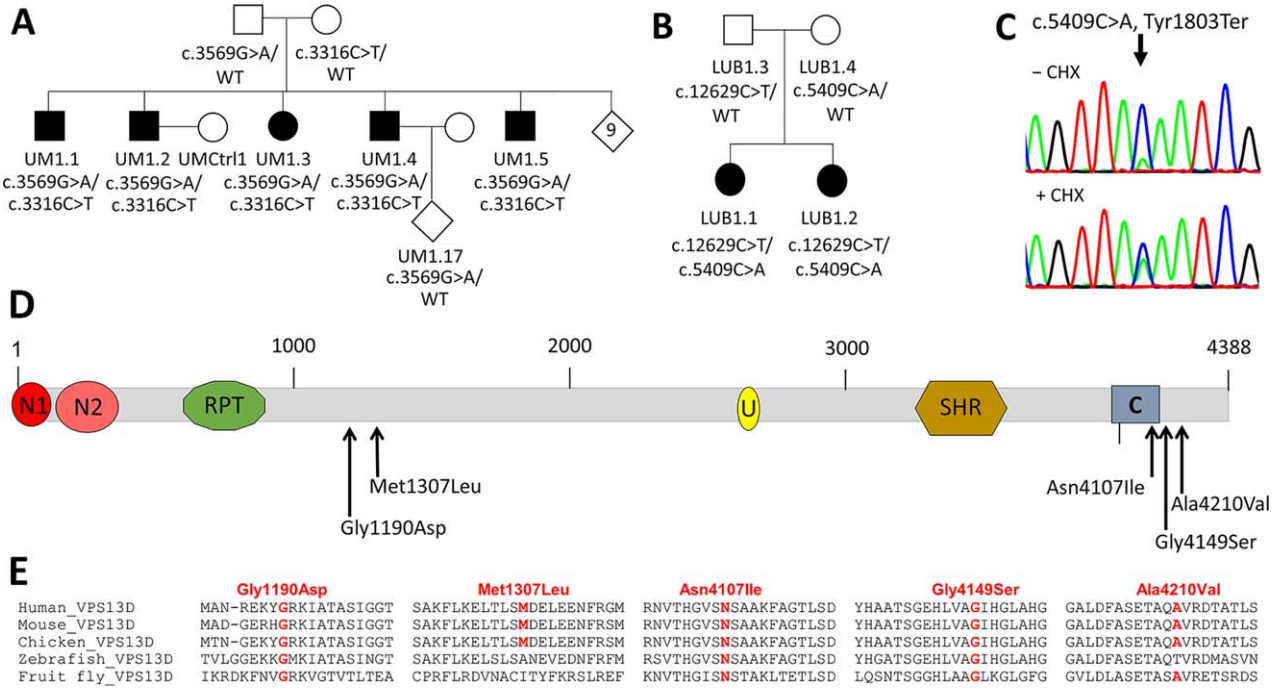

FIGURE 1: Multiplex ataxia families with compound heterozygous mutations in *VPS13D*. (A) Pedigree of Family UM1. Affected siblings are indicated by black filled symbols; unaffected individuals are marked by unfilled symbols. The 9 unaffected siblings are shown with an open diamond. Mutational status is given below each individual together with the respective laboratory ID. (B) Pedigree of Family LUB1 with mutations in the 2 affected sisters, shown by black filled symbols. (C) cDNA sequences of the c.5409C>A mutation before (top panel) and after (lower panel) treatment with cycloheximide (CHX). The traces are representative of 2 sequencing runs. The nonsense-mutated allele was stabilized and showed similar expression levels upon treatment. (D) Predicted domain maps of VPS13D protein (http://www.ebi.ac.uk/interpro/protein/Q5THJ4) with the identified missense mutations marked: N1 = VPS13 1st N-terminal domain (amino acids [aa] 2–115); N2 = VPS13 2nd N-terminal domain (aa 137–356); RPT = Repeated Coil Region; U = UBA (ubiquitin-associated)-like domain (aa 2627–2679); SHR = VPS13 short root transcription factor-binding domain (aa 3276–3558); C = VPS13 C-terminal domain (aa 3983–4129). The 5 different missense mutations appear to cluster in 2 regions, one in the middle and the other near the C domain. (E) Amino acid sequence alignments of the regions surrounding each missense mutation across various species. Whereas Gly1190Asp, Asn4107Ile, and Gly4149Ser

the expression of *VPS13D* in LUB1.1 and a control was compared to the expression of *ß-actin, HPRT*, and *YAZ*, which served as reference genes. These quantitative PCRs were performed with SYBR Green on the LightCycler 480 system (Roche Molecular Systems; data not shown). Because both quantitative PCR and sequencing indicated instability of the allele with the nonsense mutation, we treated fibroblasts of LUB1.1 with cycloheximide for 8 hours at 100 μg/ml final concentration to stabilize the transcript and confirm -NMD- as the cause. The effect of cycloheximide was evaluated by sequencing of cDNA.

In addition to nonsense and missense mutations, we detected 3 variants at splice sites (c.941 + 3A>G, c.2237-1G>C, c.9998 + 4A>C). Because we are limited in performing skin biopsy for research purposes to adults only, per our institutional review board, we do not have fibroblast cultures from the children with splice mutations. Instead, we used 2 online slice site prediction tools to estimate the impact of these variants on splicing: Human Splicing Finder (HSF; http://www.umd.be/HSF3/) [12] and Splice Site Prediction (SSP; http://www.fruitfly.org/seq_tools/splice.html), set to mammals. HSF provides a consensus value (CV) variation as output with the interpretation of CV $< -10\%$ indicating a disruption of the splice site. SSP generates a score between 0 and 1, with a score of 0.5 recognizing about 90% of the actual sites and a false-positive rate of $< 5\%$. The higher the score, the higher the probability that the splice site is active.

Comparison of Mutation Frequencies in VPS13D *Paralogs*

To assess the impact of the loss of function of each *VPS13* paralogs, we compared phenotypes of animal models available in the literature and in databases and examined estimates of mutation frequencies in humans. To assess the common mutation types (eg, loss of function, missense) in each *VPS13* paralog-associated disease, we restricted analysis to cases in which both mutations are known.

Functional Studies in Patient-Derived Fibroblasts

From the UM1 family, we established fibroblast cell lines from 2 patients (UM1.2 and UM1.4) and 2 controls (UM1.17, a

daughter of an affected, and UMCtrl1, a married-in unaffected spouse). From LUB1, fibroblast lines were established from LUB1.1, the index patient, and her heterozygous parents (LUB1.3 and LUB1.4). In addition, fibroblasts from 2 unrelated control lines (LUBCtrl1, also known as L-2132; LUBCtrl2, also known as L-2134) were used.

For mitochondrial imaging in fibroblast from the UM1 family, MitoTracker Red CMXRos (Invitrogen, Carlsbad, CA) was applied to fibroblasts cultured on coverslips for 40 minutes before fixing in 4% formaldehyde for 12 minutes. Through a PLAPON 60 × (1.42 Oil) lens on an Olympus (Tokyo, Japan) FV1000 confocal microscope, 6 to 8 Z stacks of images were obtained per visual field to produce images of in total approximately 72 to 127 cells per line. Images were flattened using Z-projection at maximum intensity using the open software Fiji,[13] which was also used to generate intensity histograms. For each 2-dimensional image, the Otsu algorithm was applied to extract the top 1% brightest pixels. To quantify spherical mitochondria, any areas smaller than 1.5 μm^2 and with less circularity than 0.18 were removed using Fiji's Analyze Particles function. The remaining selected areas correspond to bright and spherical mitochondria. The average number of such selected objects per cell was calculated in each cell line. We also computed the percentage of cells with >2 such objects in the perinuclear region. Form factor analysis as a measurement of the mitochondrial network integrity was performed by using a selection algorithm in the software program Volocity (PerkinElmer, Waltham, MA) to select mitochondrial objects (1 standard deviation above the mean MitoTracker intensity) of a projected z stack image (average intensity). For each projected image containing 4 to 12 cells, form factor, defined as $[P_m^2]/[4\pi A_m]$ with P_m being the perimeter and A_m being the area of a mitochondrion, was calculated for all selected mitochondria, and the mean was obtained for the entire image field. For each individual, 11 to 17 images from 2 independent experiments were analyzed.

In fibroblasts of Family LUB1, the form factor was determined as previously described.[14] In brief, the mitochondrial network in fibroblasts was stained with an anti-GRP75 antibody (1:1,000; Abcam, Cambridge, MA) in combination with the Zenon immunolabelling kit (Invitrogen) according to the manufacturer's protocol. Based on single cell images, mitochondria area and outline were measured and the form factor was calculated. Mean form factor was averaged over 20 cells per individual.

Measurement of the Rate of Adenosine Triphosphate Synthesis in Cultured Fibroblasts

Adenosine triphosphate (ATP) was quantified, in triplicate, using the ATP Bioluminiscence Assay Kit CLS II (Roche Diagnostics, Mannheim, Germany) following the manufacturer's instructions. ATP was measured in a luminometer (Berthold Detection Systems, Pforzheim, Germany), and calculated as ATP generated (micromoles) per minute per milligram of protein. The amount of protein was determined using the BCA Protein Assay Kit (Pierce, Rockford, IL).

Functional Studies in Drosophila *Models*

All fly lines and related constructs were purchased from the Bloomington Stock Center (Bloomington, IN), including *Vps13D* mutant lines (#56282 [$Vps13D^{11101}$] and #22996; only #56282 homozygous shown), Vps13D RNA interference (RNAi; #38320), motoneuron-specific Gal4 driver (D42-Gal4, #8816), a deficiency line Df(3L)Exel6117 (#7596), and fluorescent mitochondrial marker (UAS-mitoGFP, #42727).[15] All phenotypes observed of homozygous *Vps13D* mutant alleles were confirmed in compound heterozygous flies of the 2 alleles, and in mutant alleles over the deficiency line, which lacks a defined region of the *Drosophila* chromosome containing the entire *Vps13D* genetic locus and some neighboring genes. For staining, we used the following primary antibodies: ATP5A (Abcam ab14748), green fluorescent protein (GFP; Life Technologies, Carlsbad, CA; A-11122, 1:1,000), horseradish peroxidase (Jackson ImmunoResearch, West Grove, PA; 123-605-021, 1:1,000), and discs large (Dlg1) (Developmental Studies Hybridoma Bank, Iowa City, IA; 4f3, 1:1,000). All secondary antibodies were from Invitrogen (Alexa-conjugated 1:1,000, 2 hours, RT). Standard dissection and immunostaining procedures were used for larval tissue analysis.[16] For larval immunostaining, tissues were fixed with 4% formaldehyde for 20 minutes at room temperature prior to staining, except for anti-ATP5A staining, in which tissue was fixed with Bouin fixative for 7 minutes at room temperature. Form factor analysis of larval ventral nerve cords was performed using Volocity to select mitochondrial networks in the cell bodies of RNAi expressing motoneurons based on threshold of mitoGFP fluorescence (2.5 standard deviations above the mean fluorescence intensity) from a projected z stack image. For each cell body, an average form factor of all mitochondria was calculated.

Statistical Analyses

Differences were analyzed statistically using unpaired *t* tests, or analysis of variance with a Bonferroni–Dunn post hoc correction.

Results

Genetic Findings

OVERVIEW. In 4 different locations in the USA and Europe, we independently detected compound heterozygous *VPS13D* mutations in 7 families. The mutational spectrum included 5 nonsense, 5 missense, 1 frameshift, 1 essential, and 2 nonessential splice site mutations (Table 1). All families carried a combination of 1 loss-of-function (LOF) mutation (nonsense, frameshift, or essential splice sites) and 1 presumably milder change (missense or nonessential splice site mutation). All variants were absent or extremely rare (<13 heterozygous carriers) in the ~120,000 individuals listed in gnomAD. Among the 5 missense mutations, Gly1190Asp and Met1307Ile, found in families UM1 and NIJ1, were located in the center of the protein. The three C-terminal missense mutations detected in families LUB1, NIJ2, and NIJ3 are close to or within the C-

TABLE 1. Compound Heterozygous *VPS13D* Mutations Identified in Each Ataxia/Spasticity Family

Subject	Mutation Protein NP_056193	Mutation cDNA NM_015378	Mutation Genomic Level	CADD Score	Mutation Taster	Frequency, gnomAD	Human Splicing Finder	Splice Site Prediction
UM1	Gly1190Asp	3569G>A	chr1:12337214G>A	25	Disease causing	Not reported		
	Gln1106Ter	3316C>T	chr1:12336961C>T	39	Disease causing	Not reported		
LUB1	Ala4210Val	12629C>T	chr1:12520418C>T	34	Disease causing	0.00004039		
	Tyr1803Ter	5409C>A	chr1:12343568C>A	33	Disease causing	Not reported		
NIJ1	Met1307Leu	3919A>T	chr1:12337564A>T	19	Disease causing	0.00004885		
	Gln662Ter	1984C>T	chr1:12331062C>T	40	Disease causing	Not reported		
NIJ2	Gly4149Ser	12445G>A	chr1:12516165G>A	35	Disease causing	Not reported		
	Gln2572Ter	7714C>T	chr1:12382602C>T	51	Disease causing	Not reported		
NIJ3	Splicing ?	941 + 3A>G	chr1:12317147A>G	17	NA	Not reported	−0.83%	0.89→0.21
	Val2987GlyfsX14	8960_8961delTG	chr1:12405505delTG	35	Disease causing	Not reported		
NIJ4	Asn4107Ile	12320A>T	chr1:12476867A>T	30	Disease causing	Not reported		
	Splicing (essential)	2237-1G>C	chr1:12335881G>C	23	NA	Not reported	−31.07%	0.99→0.00
WF1	Splicing ?	9998 + 4A>C	chr1:12416585A>C	9.6	NA	0.00003738	−10.57%	0.93→0.62
	Leu2277Ter	6829delC	chr1:12371876delC	35	Disease causing	Not reported		

Coordinates of all detected mutations are based on NM_015378 for cDNA and GRCH37/hg19 built for genomic DNA. CADD score and MutationTaster are in silico prediction of deleteriousness of each mutation. Three of the mutations have been reported previously in public exome/genome databases (gnomAD: genome aggregation consortium at http://gnomad.broadinstitute.org/gene/ENSG00000048707). For splice variants, splice site prediction scores were calculated at Human Splicing Finder (http://www.umd.be/HSF3/) and Splice Site Prediction (http://www.fruitfly.org/seq_tools/splice.html).

CADD = Combined Annotation Dependent Depletion; NA = no assessment.

domain (see Fig 1D), which is conserved and unique among all VPS13 proteins including yeast.

*UM1 ATAXIA FAMILY (*SCAR4*).* We have previously reported a family with 14 siblings, 5 of whom had adult onset spinocerebellar ataxia with saccadic eye intrusion (see Fig 1A; *SCAR4*[6,7]. After exclusion of known ataxia mutations, genome-wide linkage analysis under a recessive, full penetrance model identified only a single locus with logarithm of odds (LOD) > 0, which was 20cM/ ~10Mb on chromosome 1p36 flanked by rs7538691 and rs761162 (LOD = 3.1, data not shown). Whole exome sequencing in 2 affected individuals revealed compound heterozygous mutations in *VPS13D* as the only likely genetic cause within the linked region. The variants comprised a paternally inherited missense change (c.3569G>A, p.Gly1190Asp) and a maternally inherited nonsense mutation (c.3316C>T, p.Gln1106Ter). Sanger sequencing verified segregation among all 12 siblings with available DNA samples. Sequencing of RT-PCR products from fibroblast cell lines of 2 patients demonstrated that the nonsense allele-containing mRNA product was less abundant, suggesting that it

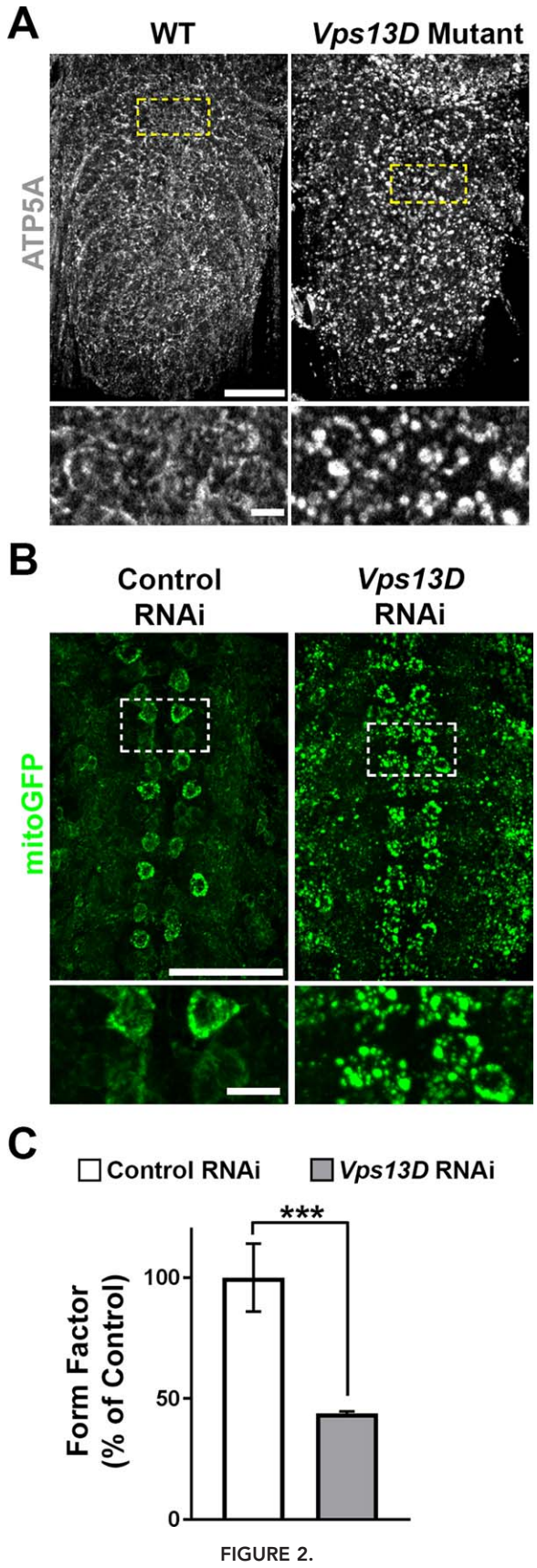

FIGURE 2.

underwent NMD (data not shown). Gly1190Asp introduces an extra negative charge and appears not to affect protein stability (data not shown).

FAMILY LUB1. In 2 affected sisters of a German family with spastic ataxia (see Fig 1B), we detected compound heterozygous mutations in *VPS13D* including a maternal nonsense mutation (Tyr1803Ter) and a paternal missense change (Ala4210Val, rs746736545). Similar to Family UM1, sequencing of cDNA of the index patient revealed the allele with the nonsense mutation to be less abundant. Treatment with cycloheximide stabilized the mutated allele and confirmed that the nonsense-mutated allele underwent NMD (see Fig 1C). NMD resulted in a decreased expression level of about 50 to 60% in Patient LUB1.1 (data not shown).

ADDITIONAL SPORADIC CASES. At the Radboudumc Expert Centre for genetic movement disorders in Nijmegen, and the genetic movement clinic in Rotterdam, the Netherlands, 4 unrelated cases of different ethnicities with compound heterozygous *VPS13D* mutations were independently identified (see Supplementary Table). NIJ1 and NIJ2 carry a combination of a nonsense mutation and a missense change, NIJ3 carries a frameshift and a nonessential splice site mutation, and NIJ4 carries an essential splice site mutation and a missense change. NIJ4 also has optic atrophy and carries a heterozygous frameshift mutation in *OPA1* (c.1156_1157del [p.Leu386Glufs*2]). A second (biallelic) mutation in *OPA1* was excluded by exome sequencing with sufficient coverage of the entire coding region and splice sites. Her mother carried the same variant and has isolated optic atrophy.

FIGURE 2: Disruption of *Vps13D* in the *Drosophila* central nervous system affects mitochondrial morphology. (A) Ventral nerve cord, stained for mitochondrial marker ATP5A, of control (w^{1118}, right panel) and *Vps13D* mutant ($Vps13D^{11101/11101}$, left panel) *Drosophila* larvae. Bottom: High-magnification single confocal z planes of areas indicated by the dashed boxes, highlighting mitochondrial morphology in neuronal cell bodies. Scale bars: 50 μm (top) and 5 μm (bottom). (B) Representative images of motoneurons (via D42-Gal4) with simultaneous expression of fluorescent mitochondrial marker mitoGFP (green) along with control (left panel) and *Vps13D* (right panel) RNAi expression. Bottom: High-magnification single confocal z planes of areas indicated by the dashed boxes, highlighting mitochondrial morphology in motoneuron cell bodies. (C) Quantification of form factor analysis of the mitochondrial network (based on mitoGFP) in neuronal cells bodies expressing control RNAi (white) versus *Vps13D* RNAi (gray); n = 50 neurons per condition (from 5 different animals). Error bars represent standard error; ***$p < 0.001$ (Student *t* test). WT = wild type. [Color figure can be viewed at www.annalsofneurology.org]

At the Wake Forest School of Medicine, Winston-Salem, North Carolina, 1 additional case, WF1, was identified by clinical exome sequencing (GeneDx). WF1 displayed hypotonia, balance and coordination difficulties, and global developmental delay; more formal clinical ataxia tests were difficult to perform, due to her current age and disease features as well as global developmental delay. WF1 has a combination of a nonsense mutation and a nonessential splice site change.

To estimate the impact of the splice site changes on the transcript, we used 2 different in silico splice site prediction programs. As expected, both programs, HSF and SSP, strongly predicted an effect on splicing of the variant at the invariant acceptor splice site of intron 18 in NIJ4, c.2237-1G>C (see Table 1), which hence was classified as LOF. The splice region variants in NIJ3 and WF1, however, are not within invariant splice consensus sites. For c.9998 + 4>C in intron 49, CV variation was −10.57%, just below HSF's −10 cutoff. SSP's prediction score dropped from 0.93 to 0.62, suggesting a mild, if any, impact on recognition of this splice site. For c.941 + 3A>G in intron 9, the CV variation was −0.83% by the HSF algorithm and would argue against an effect on splicing. However, the SSP score dropped from 0.89 to 0.21, suggesting reduction in predicted splicing ability. These 2 nonessential splice site mutations are hence not considered complete LOF alleles, as they may allow some correctly spliced transcripts. Confirmatory analysis of intronic splice region variants could not be performed at this time (see Materials and Methods for details).

Clinical Findings

All cases except for WF1, which was too young, had either ataxia or spasticity as a core symptom. Onset ranged from infancy to adulthood. The UM1 family, previously designated as *SCAR4*, demonstrated primarily adult onset ataxia with distinct macrosaccadic intrusions,[7] with pyramidal features, neuropathy, and myoclonus but no intellectual disability.[6] Videos of the clinical examinations and the distinct eye phenotype are available in the online supplement of Swartz et al.[7] The 2 sisters from Family LUB1 were similar to UM1 in their onset and clinical phenotypes, except for a different oculomotor phenotype. By contrast, NIJ1 had a much earlier onset (<5 years) and symptoms were more debilitating (wheelchair-bound by age 17 years). Whether his phenotypic difference originates from more severe *VPS13D* mutations or other environmental or genetic factors is unknown at this time. Similarly, NIJ4 and WF1 were severely affected with an age at onset in the first year of life. In addition to ataxia and neuropathy, NIJ4 suffers from developmental delay, seizures, and optic atrophy. Coincidentally, she carries an additional mutation in *OPA1* (optic atrophy 1/ mitochondrial dynamin-like GTPase), which explains the optic atrophy but not the additional seizures and the developmental delay. NIJ2 was affected by spastic paraplegia without ataxia, with onset in early adulthood. Patients WF1 and NIJ3 might be more severely affected due to 2 severe mutations including a nonessential splice site change and an LOF mutation, in contrast to the combination of a missense and an LOF mutation in the other subjects.

Among VPS13 *Paralogs,* VPS13D *Is the Most Intolerant to Mutations*

Yeast *vps13* is implicated in many cellular functions including sporulation, Golgi organization, and mitochondrial integrity.[17] During metazoan evolution, 2 duplication events gave rise to 3 paralogs: *VPS13A/C, B, and D. Drosophila* Vps13 (CG2093) is an ortholog of *VPS13A/C*, which further duplicated in the vertebrate evolution into *VPS13A* and *VPS13C* (updated from Velayos-Baeza et al[18]). Because not much is known about *VPS13D*-specific function, we compared reported phenotypes of VPS13 homologs in the 2 model organisms fly and mouse (fly: CG2093[19]; mouse: MGI2444304,[20] MGI2444207, and MGI2448530; Table 2). Mutations in *Vps13D*/*VPS13D* cause embryonic lethality in both animals, whereas mutations in *VPS13A* and *C* appear more tolerable during early development (animal phenotypes for *VPS13B* are unavailable).

A similar trend was observed in human populations (see Table 2). Residual Variation Intolerance Score (RVIS) is a gene-based intolerance score derived from allele frequency in whole exome sequence data.[21] Among the paralogs, *VPS13D* has the lowest RVIS score of −4.23, 0.14 percentile, suggesting that *VPS13D* is among the most mutation-intolerant of human genes. We also compared the frequency of LOF in each paralog in the Exome Aggregation Consortium (ExAC) browser. Again, *VPS13D* emerges as most sensitive to LOF mutations, with the lowest ratio of the number of variants observed over expected. For *VPS13D*, the probability of LOF intolerance (pLI) score is 1, virtually certain. Chorea acanthocytosis is caused in 29 of 31 cases by LOF/LOF mutations in *VPS13A*,[22] Cohen syndrome in 41 of 45 cases by LOF/LOF mutations in *VPS13B*,[23–27] and Parkinson disease in 3 of 4 cases by LOF/LOF mutations in *VPS13C* cases.[28,29] In summary, *VPS13D* is intolerant to complete LOF of both alleles, being likely incompatible with life, consistent with our finding of only compound heterozygous missense/LOF or nonessential splice/LOF mutations.

TABLE 2. Mutations of *VPS13D* Paralogs in Animals and Humans

			Mutation Intolerance in Humans				Human Disorder	
Yeast Cellular Functions Implicated	Fruit Fly Paralogs, Mutant Phenotypes	Vertebral Paralogs Mouse Null Phenotypes	RVIS	%ExAC v2 RVIS	LoF O/E	LoF pLI	Disorder	Disease Mutation Type
		VPS13A viable, acanthocytosis, neurologically abnormal in 129/SvEv background[20]	−1.85 (2.03%)	−3.75 (0.51%)	30/119.0	0.00	Chorea acanthocytosis[22]	1/31 MIS/MIS 1/31 MIS/LOF+ 29/31 LOF+/LOF+
	Vps13/ CG2093,[19] reduced life span, neuro-degeneration							
Vps13,[17] sporulation, integrity of mitochondria, Golgi organization, organelle junction		***VPS13C*** viable, Neurologically normal[c]	−0.61 (17.5%)	−2.83 (1.20%)	83/141.1	0.00	Parkinson disease[28,29]	1/4 MIS/LOF+ 3/4 LOF+/LOF+
	Vps13B/ CG15523, no data available	***VPS13B*** no data available	−0.81 (12.08%)	−2.13 (2.69%)	65/127.8	0.00	Cohen syndrome[23–27]	3/45 MIS/MIS 1/45 MIS/LOF+ 41/45 LOF+/LOF+
	Vps13D/ CG32113,[b] embryonic lethality, mitochondrial defects	***VPS13D*** embryonic lethality before placentation with complete penetrance[d]	−4.23 (0.14%)	−5.77 (0.11%)	28[a]/156.2	1.00	Ataxia/Spasticity[b]	5/7 MIS/LOF+ 2/7 splice?/LOF+

Residual Variation Intolerance Score (RVIS) is a mutation intolerance score (more negative, more intolerant) and its percentile rank in all human genes is given in parenthesis (lower, more intolerant). %ExAC v2 RVIS is RVIS v4, constructed on ExAC v2 (gnomAD) release. LoF (Loss of function) represents stop-gained and essential splice site mutations as defined in ExAC. LoF O/E represents the ratio of the number of variants observed over expected. LoF pLI is the probability of LoF Intolerance (pLI >=0.9 regarded as extremely LoF intolerant). RVIS, LoF O/E and pLI are based on ExAC. LOF indicates LoF plus frameshift mutations and LOF+ includes large deletions and insertions as well.

[a]For *VPS13D*, gnomAD lists 65 LOF variants, with no increased frequency in any particular geographic/ethnic population.

[b]This study.

[c]MGI2444207.

[d]MGI2448530.

ExAC = Exome Aggregation Consortium; MIS = missense.

Vps13D *Disruption in* Drosophila *Is Lethal and Causes Mitochondrial Defects*

Known also as CG32113 in flies, fly *Vps13D* shows 33% protein identity to the human gene (see Table 2). Consistent with *Vps13d* lethality in mice, flies disrupted for *Vps13D* do not survive beyond the 2nd instar larvae stage. This lethality was confirmed with 2 independent lines containing large insertions in the coding region of *Vps13D*, including compound heterozygous animals containing 1 copy of each *Vps13D* allele, hence ruling out secondary mutations as the cause of lethality.

While we observed no obvious defects in markers for Golgi, endoplasmic reticulum, lysosomes, and the nucleus (data not shown), we observed that deletion of *Vps13D* led to severe alterations in mitochondrial morphology. In early 2nd instar larvae before lethality, instead of forming fine mitochondrial networks in individual cells, mitochondria appear as singular, enlarged objects. This abnormal mitochondrial appearance was present in the larval brain (see Fig 2A) and other tissues in these young larvae (not shown).

We then used RNAi-mediated knockdown[30] to inhibit expression of *Vps13D* specifically in motoneurons. This allows for survival of larvae to the 3rd instar stage (death at pupal stage), which enables further characterization of *Vps13D*'s autonomous function in neurons. By coexpression of mitoGFP targeted specifically to

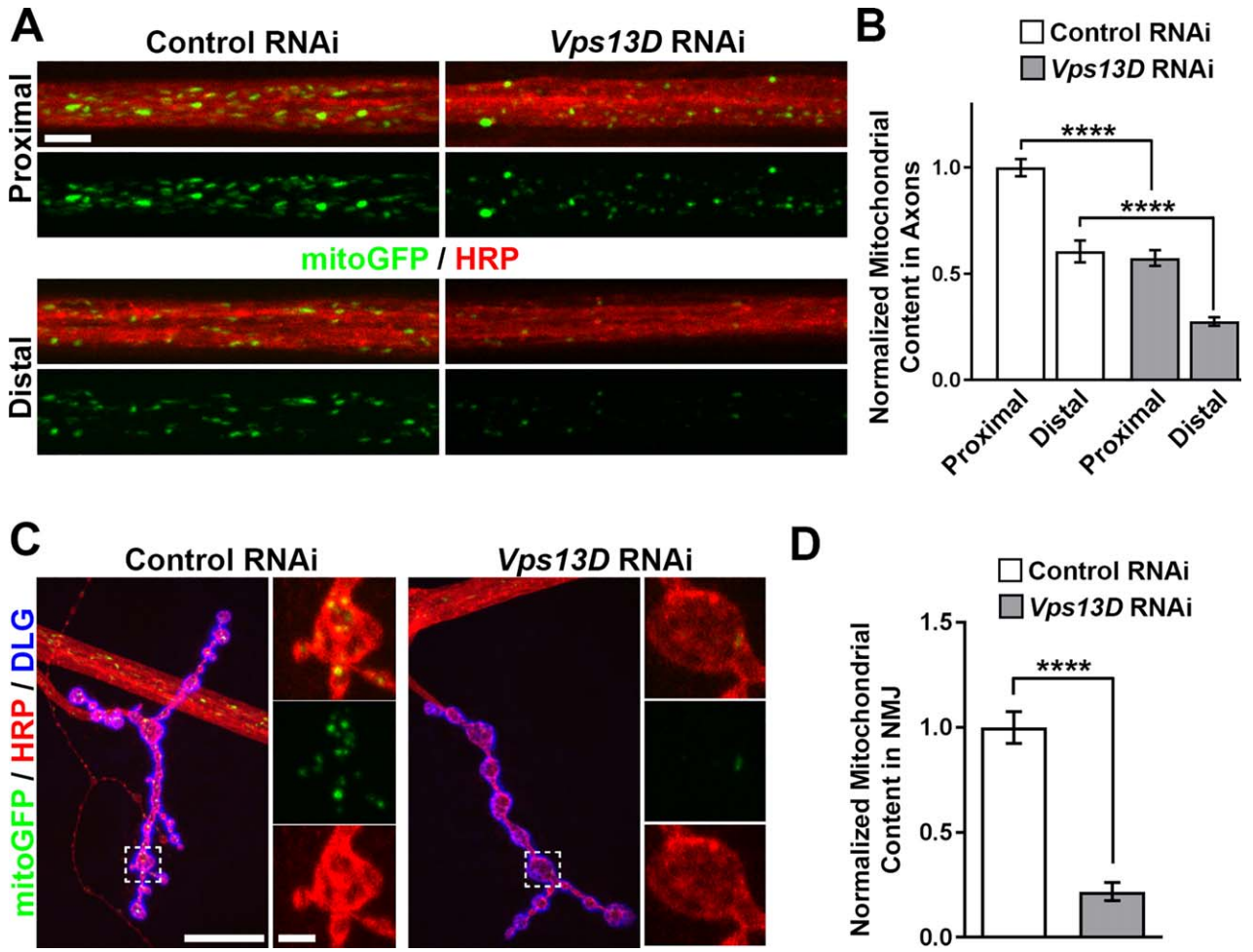

FIGURE 3: Knockdown of *Vps13D* in *Drosophila* motoneurons disrupts the distribution of mitochondria to distal axons. (A) Segmental nerves (horseradish peroxidase [HRP], red) containing motoneuron axons expressing fluorescent mitochondrial marker mitoGFP (green) of control RNAi and *Vps13D* RNAi knockdown (RNAi) animals. Nerves near the ventral nerve cord (VNC; proximal, top) and distant from the VNC (distal, bottom) are shown. Scale bar: 10 μm. (B) Quantification of the mitochondrial content per area within segmental nerves in proximal and distal regions of motoneurons expressing control RNAi (white) versus *Vps13D* RNAi (gray). Data are normalized to the control RNAi proximal region condition; n ≥ 10 individual nerves from 5 different animals. Error bars represent standard error; ****$p < 0.0001$ (Student *t* test). (C) Larval neuromuscular junction (NMJ) synapses from motoneuron axons expressing fluorescent mitochondrial marker mitoGFP (green) of control and *Vps13D* RNAi knockdown animals. HRP (red) labels neuronal membrane, whereas DLG (disc large 1, blue) labels NMJ postsynaptic region. High-magnification images of the synaptic region (indicated by the dashed box) are shown (right panels) to highlight mitochondria occupying the synaptic region. Scale bars: 20 μm (left) and 2.5 μm (right). (D) Quantification of the mitochondrial content in the NMJ synapse per area of motoneurons expressing control RNAi (white) versus *Vps13D* RNAi (gray). Data are normalized to the control RNAi condition; n = 5 animals (each n represents the average mitochondrial content of ≥6 NMJ synapses/animal). Error bars represent standard error; ****$p < 0.0001$ (Student *t* test).

mitochondria of the RNAi-depleted neurons,[15] we observed enlarged spherical mitochondria (see Fig 2B). Compared to a control RNAi line targeting luciferase, knockdown by Vps13D RNAi resulted in a significant reduction in quantified form factor (see Fig 2C), consistent with a loss of complexity of the mitochondria network coinciding with enlarged, isolated mitochondria. These observations suggest a role for *Vps13D* in regulating mitochondrial morphology and potentially also mitochondrial function in neurons.

The abnormal mitochondrial network in neuronal cell bodies led us to hypothesize that loss of Vps13D would deleteriously impact the distribution of mitochondria to distal regions of neurons.

Previous studies have linked deficiencies in mitochondrial trafficking to distal neurites in neurodegenerative diseases and neuropathies.[31,32] We observed that reduction of Vps13D in motoneurons led to strong impairment in the distribution of mitochondria in peripheral axons in segmental nerves and neuromuscular junction synapses (Fig 3). The density of mitochondria was progressively reduced concomitant with increased distance from the cell body locations in the central nervous system. This failure to distribute mitochondria

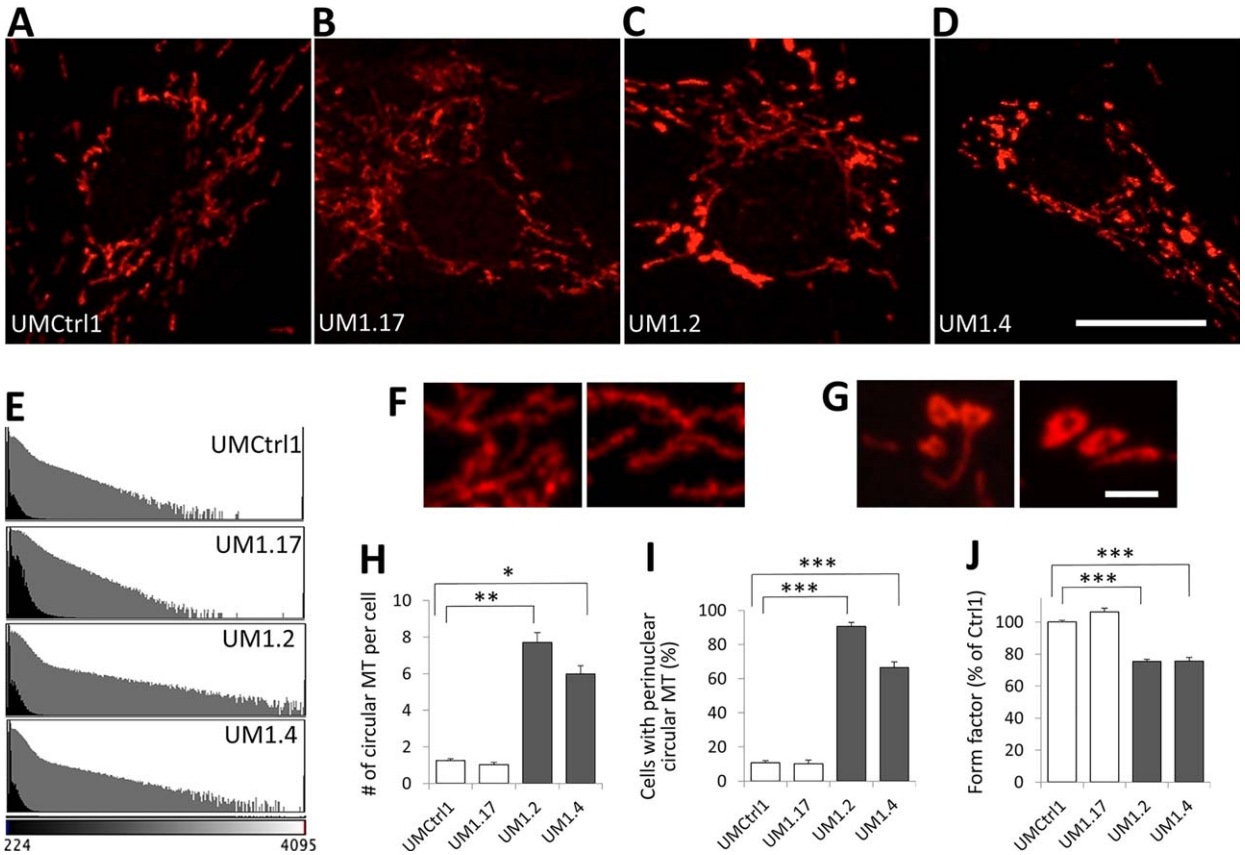

FIGURE 4: Patient fibroblasts Family UM1 contain abnormal spherical mitochondria. (A–D) Comparison of mitochondria in 4 fibroblast lines of Family UM1 stained with MitoTracker. (A) UMCtrl1: wild type for *VPS13D*. (B) UM1.17: asymptomatic heterozygous carrier of the Gly1190Asp missense mutation. (C, D) UM1.2 and UM1.4: VPS13D compound heterozygous patients. Note that whereas the majority of the mitochondria in the control cells are elongated and of similar intensity, the patient cells are loaded with particularly bright, circular mitochondrial objects mostly localized in the perinuclear region. (E) Intensity histogram of MitoTracker images. The x-axis represents the intensity; the numbers of pixels are plotted on the y-axis (the black plots in natural number scale and the gray plots in log scale). Note that both patients have many more pixels with higher intensity, indicative of the increase in bright MitoTracker-stained objects. (F, G) Perinuclear mitochondria at higher magnification (60 × lens, 4 × zoom). Control mitochondria (F; UMCtrl1) are elongated, tubular, and interconnected, whereas the patient mitochondria (G; UM1.2) are often donut-shaped. Here, brightness was individually optimized to reveal the structural details and is not comparable. Scale bars: 20 μm (A–D) and 2 μm (F, G). (H) Average number of circular mitochondrial (MT) objects identified by image processing. Such circular objects are present in the control cell lines at low frequencies but become much more abundant in the affected cell lines (~6-fold increase). (I) Percentage of cells with at least 3 perinuclear circular MT objects. The patient fibroblast cultures have a higher number of cells with perinuclear circular MT objects than control (6- and 9-fold increase). (J) Form factor analysis of the mitochondrial network stained by MitoTracker. In H–J, error bars represent standard error; *$p<10^{-4}$, **$p<10^{-5}$, and ***$p<10^{-6}$ (Student *t* test). [Color figure can be viewed at www.annalsofneurology.org]

resembles previously described defects for mutations in mitochondrial fission/fusion machinery.[31]

Patient-Derived Fibroblasts Show Altered Mitochondrial Morphology

Given these fly data, we also investigated mitochondrial function and morphology in human fibroblasts. Staining fibroblasts from the affected subjects of family UM1 with MitoTracker, which accumulates in mitochondria in a membrane potential–dependent manner, revealed significantly brighter mitochondria (Fig 4). Whereas the typical mitochondrial network of elongated objects and branches was observed in both control and patient cells, the perinuclear regions of only affected cells often contained unusually bright and significantly more spherical mitochondrial objects, which were mostly in clusters and at higher magnification appeared to be donut-shaped. To quantify the abundance of the bright and spherical mitochondria in each cell line, we extracted the top 1% brightest pixels from each image and selected circular objects based on computed circularity score. The average number of such abnormal mitochondrial objects was ~6-fold higher in the affected compared to control cells. In the perinuclear region, such objects were identified in clusters (≥3) in ~10% of normal but 91% and 67% of fibroblasts of affected subjects' cells. Consistent with the *Drosophila* data, form factor analysis

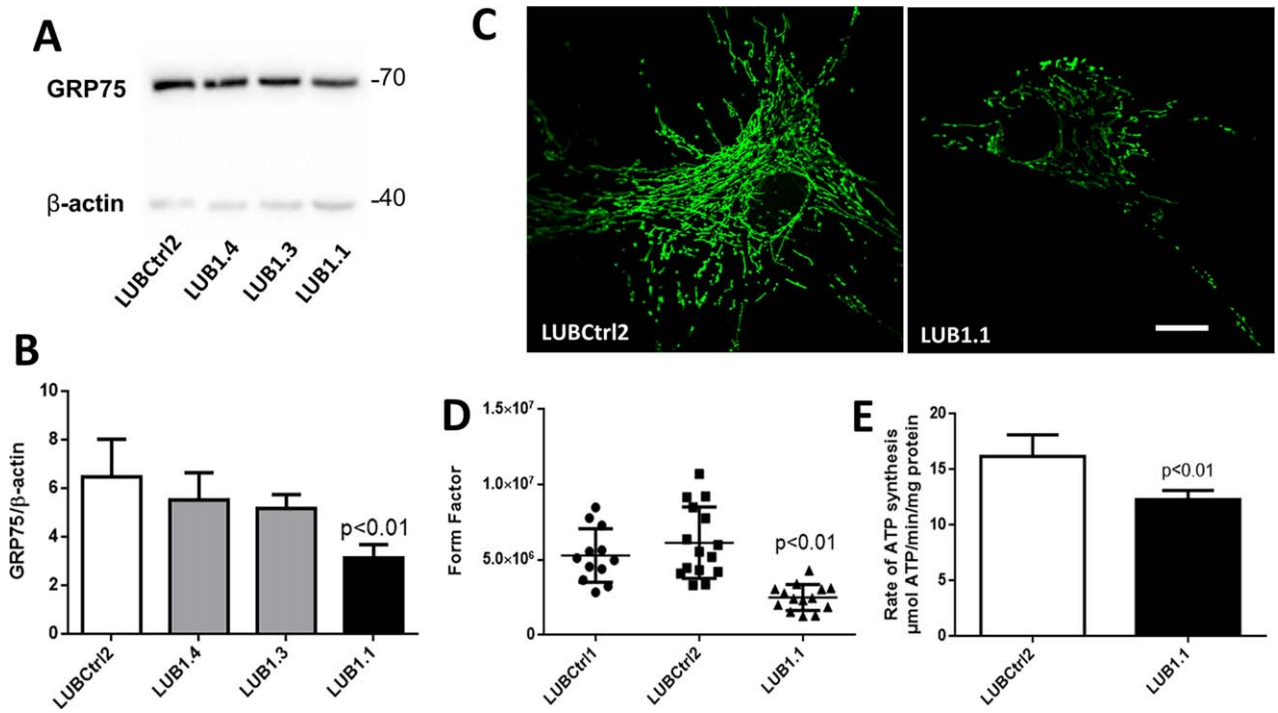

FIGURE 5: Altered mitochondrial morphology and decreased adenosine triphosphate (ATP) in *VPS13D* mutant fibroblasts of Family LUB1. (A) Western blot analysis shows mitochondrial GRP75 protein levels in the *VPS13D* mutant fibroblasts (LUB1.1), patient's parents (LUB1.3 and LUB1.4), and healthy control fibroblasts (LUBCtrl2) with *β*-actin as loading control. (B) Quantification of the above GRP75 Western blot using ImageJ. (C) The mitochondrial network was investigated under basal conditions by confocal microscopy in fixed cells immunostained with anti-GRP75. Scale bar: 20 μm. (D) Form factor as a measure for mitochondrial interconnectivity (GRP75 immunostaining) was calculated for 2 control fibroblast lines (LUBCtrl1, LUBCrtl2) and 1 patient line (LUB1.1). Each dot represents measurement in a single cell (n = 20). The mean values and the standard deviations of the investigated individuals are shown. (E) ATP production was determined based on luminescence. ATP concentration (micromoles) was calculated per minute per milligram of protein (n = 3 independent experiments). In B and E, the error bars indicate the standard error of the mean of n ≥ 3 independent experiments. [Color figure can be viewed at www.annalsofneurology.org]

also revealed a significant reduction in the degree of mitochondrial branching in the affected fibroblasts compared to controls. These observations suggest structural defects in mitochondria in VPS13D-deficient fibroblasts.

Independent analysis of fibroblasts of the proband of family LUB1 demonstrated that the affected fibroblasts expressed reduced levels of mitochondrial GRP75 protein compared to controls (Fig 5). Form factor analysis of GRP75 immunostaining revealed a similar reduction in the degree of mitochondrial branching of proband fibroblasts compared to 2 unrelated healthy controls. These structural mitochondrial changes were accompanied by a reduced ATP production rate of LUB1.1 compared to control fibroblasts.

Discussion

In this study, we have identified 7 different compound heterozygous mutations in *VPS13D* in 12 patients and have linked VPS13D/Vps13D defects in patient fibroblasts and in flies to mitochondrial deficits. Our study also included a large family with ataxia (*SCAR4*) and linkage to a 10Mb region on chromosome 1p36 harboring the *VPS13D* gene.

The core phenotype of the 11 patients older than 2 years with compound heterozygous *VPS13D* mutations is characterized by movement disorders of the ataxia-spasticity spectrum, ranging from predominant ataxia, spastic ataxia, to spastic paraplegia without ataxia, and ataxia plus phenotypes. The latter included 2 cases with an additional developmental delay phenotype (NIJ3 and NIJ4). The youngest patient, WF1 of age 2 years at the last evaluation, presented with hypotonia and developmental delay, including motor delay, and was not yet ambulatory. These 3 patients also have different types of or additional mutations, as NIJ3 and WF1 carry nonessential splice region variants in addition to an LOF. This may be more severe than the combination of missense/LOF found in the other cases. In addition, NIJ4's presentation may be complicated by an additional mutation in *OPA1*. The protein encoded by *OPA1* is also implicated in mitochondrial function. It is conceivable that there may be an interactive effect of the 2 mutated genes linked to mitochondrial dysfunction. Interestingly, recent data have shown that about 5% of patients carry 2 independent Mendelian diseases.[33] However, digenic inheritance cannot be ascertained based on this single case. Of note, homozygous

or compound heterozygous *OPA1* mutations cause an extended multisystem phenotype that includes ataxia and spastic paraplegia, known as Behr syndrome.[34] Although there was complete coverage of the *OPA1* coding regions and splice sites, no second mutation in the *OPA1* gene was detected by exome nor by copy number analyses (conducted as described).[35] Hence, although we cannot exclude an undetected intronic or promoter mutation that is not penetrant, as the father does not have optic atrophy, we believe Behr syndrome as an alternative diagnosis in this case is not likely.

The overlap between genetic forms of ataxias and hereditary spastic paraplegias is well recognized, as there are other examples of genes (eg, *SPG7*) that when mutated can give rise to either pure ataxia or spastic paraplegia or to a mixed phenotype of spastic ataxia,[36,37] developmental delay, and seizures, and other complex phenotypes commonly accompany early onset recessive ataxias.[2] In addition, there was variability in age of onset in our patients, which is also not unusual for ataxias. Frequently observed neurological comorbidities in our series included peripheral axonal neuropathy and extrapyramidal signs such as myoclonus and dystonia. Infertility was noted in 2 male cases. Although it is currently uncertain whether this is *VPS13D*-related, infertility is a known feature of mitochondrial disease.[38]

VPS13D encodes a large protein (4,388 amino acids), whose paralogs cause other neurological disorders; *VPS13A* mutations cause chorea acanthocytosis, characterized by a severe hyperkinetic movement disorder, myopathy, epileptic seizures, cognitive decline, and behavioral changes,[22,39] and perturb protein homeostasis in the fly.[19] *VPS13B* is involved in Cohen syndrome[40,41] and *VPS13C* in rare cases of genetic Parkinson disease with mitochondrial dysregulation and mitophagy.[28] Most of these disease-associated mutations are LOF/LOF (see Table 2). In contrast to the other VPS13 paralogs, knocking out *VPS13D's* homologs in *Drosophila* (our results) and mouse (MGI:2448530) leads to embryonic lethality, and not a single LOF/LOF mutation was identified, suggesting that some residual VPS13D function in humans may be critical for survival. In addition, the ExAC server's pLI score, that is, the probability that a gene may be intolerant to haploinsufficiency, for *VPS13D* is 1, in contrast to all other *VPS13* genes (see Table 2).[42] We did not, however, observe the predicted intolerance to haploinsufficiency, as 1 parent of each of the cases reported here was haploinsufficient, but none was symptomatic, including 1 parent who lived into their 90s without apparent neurological problems.

Our genetic data allow for some first, yet cautious speculations on genotype–phenotype correlations. First, our current data collectively point to missense/LOF mutations tending to cause relatively pure ataxia and/or spasticity. Second, as suggested by the more severe NIJ3 and WF1 cases, who carry nonessential splice site/LOF mutations, other mutation type combinations may be associated with a broader and/or more severe spectrum of phenotypes. Lastly, the other severe case, NIJ4, had a coexistent dominant *OPA1* mutation and corresponding optic atrophy,[43] which was also observed in the subject's mother. The *OPA1* mutation may contribute epistatically to the phenotype, as *OPA1* also affects mitochondrial function.[43]

Although our study convincingly establishes missense/LOF mutations in *VPS13D* as causing ataxia/spastic paraplegia and mitochondrial pathology, many questions remain to be addressed. Clinically, predicting the phenotype from new mutations in *VPS13D* will be difficult. Even for missense/LOF mutation carriers, the clinical presentation varied in our series. In addition, homozygous or compound heterozygous missense mutations were not observed here. As *VPS13D* is a large gene with many missense variants reported in databases including homozygosity,[42] it will be even more difficult to predict pathogenicity of any novel biallelic missense variants.

Although further work is warranted to pin down the precise mitochondrial defect, we have shown abnormal mitochondrial morphology in both flies and patient cell lines, and reduced mitochondrial function in fibroblasts. Mitochondrial dysfunction is associated with several other ataxias and spastic paraplegias such as Friedreich ataxia,[44] *SCA28*,[45] *POLG*,[46] and *SPG7*,[47] as well as in some unexplained ataxias.[48] Although we observed a defect in mitochondrial distribution in both *Drosophila* neurons lacking Vps13D and patient fibroblasts containing mutations in *VPS13D*, the precise biological underpinnings of this defect are still under investigation, including electron microscopy studies to assess mitochondrial morphology. Alterations of mitochondrial dynamics such as transport, fission, and/or fusion[31] can all potentially manifest in aberrant distribution of mitochondria throughout the cell. Various mutations in mitochondrial genes lead to the production of reactive oxygen species,[49] which can additionally disrupt mitochondrial distribution in neurons. Combining the in vitro cellular model of patient fibroblasts and neurons differentiated from induced pluripotent stem cells with in vivo experiments in the genetic fly model may help us parse out the cellular role of VPS13D in mitochondrial biology and disease progression. These methods will also allow for testing of potential therapies that target mitochondrial dysfunction and that could be common to other forms of ataxia and spastic paraplegias.

While this article was under review, Anding et al published findings showing VPS13D to be a ubiquitin-binding protein affecting mitochondrial fission and fusion,[50] consistent with our findings, and also implemented VPS13D in autophagy, a process that we have recently reported to be involved in ataxia.[51]

Acknowledgment

This work was supported by the NIH-NINDS (NS078560, M.B.; NS069844, C.C.; F32NS098611, RI), the National Ataxia Foundation (M.B.), the European Union's Horizon 2020 research innovation program under ERA-NET Cofund action 643578, ZonMW (9003037604; B.P.v.d.W.) under the framework of the E-Rare-3 network PREPARE, the Hersenstichting (B.P.v.d.W.), Radboud University Medical Center (B.P.v.d.W.), Bioblast Pharma (B.P.v.d.W.), the Foundation of the University Hospital Schleswig-Holstein ("Gutes Tun!"; A.M. and K.L.), and a career development award from the Hermann and Lilly Schilling Foundation (C.K.).

We thank the patients for their willingness to participate and their patience during our research; Dr P. Capetian for clinical evaluation of Family LUB1 and for referring to the study; L. Gates, T. Kubisiak, and F. Hinrichs for excellent technical assistance; Dr J. Gudjonsson for fibroblast biopsies; S. Cho for useful discussion on VPS13 evolution; and Drs B. Post, J. Schieving, M. Jongen, and A. Shaikh for providing important clinical data.

Author Contributions

J.Z.L., A.M., V.S., C.K., C.C., K.L., B.P.v.d.W., and M.B. contributed to the conception and design of the study. E.Se., R.I., M.D., E.-J.K., J.T., N.B., E.Sa., S.L., A.B.O., T.J., and A.J.A.K. contributed to acquisition and analysis of data. E.Se., R.I., M.D., E.-J.K., C.K., C.C., K.L., B.P.v.d.W., and M.B. contributed to drafting the text and preparing the figures.

Potential Conflicts of Interest

Nothing to report.

References

1. Sandford E, Burmeister M. Genes and genetic testing in hereditary ataxias. Genes (Basel) 2014;5:586–603.
2. Beaudin M, Klein CJ, Rouleau GA, Dupre N. Systematic review of autosomal recessive ataxias and proposal for a classification. Cerebellum Ataxias 2017;4:3.
3. Marras C, Lang A, van de Warrenburg BP, et al. Nomenclature of genetic movement disorders: recommendations of the International Parkinson and Movement Disorder Society task force. Mov Disord 2017;32:724–725.
4. Fogel BL, Lee H, Deignan JL, et al. Exome sequencing in the clinical diagnosis of sporadic or familial cerebellar ataxia. JAMA Neurol 2014;71:1237–1246.
5. Synofzik M, Schule R. Overcoming the divide between ataxias and spastic paraplegias: shared phenotypes, genes, and pathways. Mov Disord 2017;32:332–345.
6. Swartz BE, Burmeister M, Somers JT, et al. A form of inherited cerebellar ataxia with saccadic intrusions, increased saccadic speed, sensory neuropathy, and myoclonus. Ann N Y Acad Sci 2002;956:441–444.
7. Swartz BE, Li S, Bespalova I, et al. Pathogenesis of clinical signs in recessive ataxia with saccadic intrusions. Ann Neurol 2003;54:824–828.
8. Sobreira N, Schiettecatte F, Valle D, Hamosh A. GeneMatcher: a matching tool for connecting investigators with an interest in the same gene. Hum Mutat 2015;36:928–930.
9. Abecasis GR, Cherny SS, Cookson WO, Cardon LR. Merlin—rapid analysis of dense genetic maps using sparse gene flow trees. Nat Genet 2002;30:97–101.
10. Trujillano D, Bertoli-Avella AM, Kumar Kandaswamy K, et al. Clinical exome sequencing: results from 2819 samples reflecting 1000 families. Eur J Hum Genet 2017;25:176–182.
11. van de Warrenburg BP, Schouten MI, de Bot ST, et al. Clinical exome sequencing for cerebellar ataxia and spastic paraplegia uncovers novel gene-disease associations and unanticipated rare disorders. Eur J Hum Genet 2016;24:1460–1466.
12. Desmet FO, Hamroun D, Lalande M, et al. Human Splicing Finder: an online bioinformatics tool to predict splicing signals. Nucleic Acids Res 2009;37:e67.
13. Schindelin J, Arganda-Carreras I, Frise E, et al. Fiji: an open-source platform for biological-image analysis. Nat Methods 2012;9:676–682.
14. Grunewald A, Voges L, Rakovic A, et al. Mutant Parkin impairs mitochondrial function and morphology in human fibroblasts. PLoS One 2010;5:e12962.
15. Pilling AD, Horiuchi D, Lively CM, Saxton WM. Kinesin-1 and Dynein are the primary motors for fast transport of mitochondria in Drosophila motor axons. Mol Biol Cell 2006;17:2057–2068.
16. Klinedinst S, Wang X, Xiong X, et al. Independent pathways downstream of the Wnd/DLK MAPKKK regulate synaptic structure, axonal transport, and injury signaling. J Neurosci 2013;33:12764–12778.
17. Myers MD, Payne GS. Vps13 and Cdc31/centrin: puzzling partners in membrane traffic. J Cell Biol 2017;216:299–301.
18. Velayos-Baeza A, Vettori A, Copley RR, et al. Analysis of the human VPS13 gene family. Genomics 2004;84:536–549.
19. Vonk JJ, Yeshaw WM, Pinto F, et al. Drosophila Vps13 is required for protein homeostasis in the brain. PLoS One 2017;12:e0170106.
20. Tomemori Y, Ichiba M, Kusumoto A, et al. A gene-targeted mouse model for chorea-acanthocytosis. J Neurochem 2005;92:759–766.
21. Petrovski S, Gussow AB, Wang Q, et al. The intolerance of regulatory sequence to genetic variation predicts gene dosage sensitivity. PLoS Genet 2015;11:e1005492.
22. Dobson-Stone C, Velayos-Baeza A, Jansen A, et al. Identification of a VPS13A founder mutation in French Canadian families with chorea-acanthocytosis. Neurogenetics 2005;6:151–158.
23. Hennies HC, Rauch A, Seifert W, et al. Allelic heterogeneity in the COH1 gene explains clinical variability in Cohen syndrome. Am J Hum Genet 2004;75:138–145.

24. Katzaki E, Pescucci C, Uliana V, et al. Clinical and molecular characterization of Italian patients affected by Cohen syndrome. J Hum Genet 2007;52:1011–1017.
25. Kolehmainen J, Wilkinson R, Lehesjoki AE, et al. Delineation of Cohen syndrome following a large-scale genotype-phenotype screen. Am J Hum Genet 2004;75:122–127.
26. Seifert W, Holder-Espinasse M, Kuhnisch J, et al. Expanded mutational spectrum in Cohen syndrome, tissue expression, and transcript variants of COH1. Hum Mutat 2009;30:E404–E420.
27. Seifert W, Holder-Espinasse M, Spranger S, et al. Mutational spectrum of COH1 and clinical heterogeneity in Cohen syndrome. J Med Genet 2006;43:e22.
28. Lesage S, Drouet V, Majounie E, et al. Loss of VPS13C function in autosomal-recessive parkinsonism causes mitochondrial dysfunction and increases PINK1/Parkin-dependent mitophagy. Am J Hum Genet 2016;98:500–513.
29. Schormair B, Kemlink D, Mollenhauer B, et al. Diagnostic exome sequencing in early-onset Parkinson's disease confirms VPS13C as a rare cause of autosomal-recessive Parkinson's disease. Clin Genet 2018;93:603–612.
30. Dietzl G, Chen D, Schnorrer F, et al. A genome-wide transgenic RNAi library for conditional gene inactivation in Drosophila. Nature 2007;448:151–156.
31. Baloh RH. Mitochondrial dynamics and peripheral neuropathy. Neuroscientist 2008;14:12–18.
32. Yu Y, Lee HC, Chen KC, et al. Inner membrane fusion mediates spatial distribution of axonal mitochondria. Sci Rep 2016;6:18981.
33. Posey JE, Harel T, Liu P, et al. Resolution of disease phenotypes resulting from multilocus genomic variation. N Engl J Med 2017; 376:21–31.
34. Carelli V, Sabatelli M, Carrozzo R, et al. 'Behr syndrome' with OPA1 compound heterozygote mutations. Brain 2015;138(pt 1): e321.
35. Pfundt R, Del Rosario M, Vissers L, et al. Detection of clinically relevant copy-number variants by exome sequencing in a large cohort of genetic disorders. Genet Med 2017;19:667–675.
36. de Bot ST, Willemsen MA, Vermeer S, et al. Reviewing the genetic causes of spastic-ataxias. Neurology 2012;79:1507–1514.
37. van Gassen KL, van der Heijden CD, de Bot ST, et al. Genotype-phenotype correlations in spastic paraplegia type 7: a study in a large Dutch cohort. Brain 2012;135(pt 10):2994–3004.
38. Demain LA, Conway GS, Newman WG. Genetics of mitochondrial dysfunction and infertility. Clin Genet 2017;91:199–207.
39. Tomiyasu A, Nakamura M, Ichiba M, et al. Novel pathogenic mutations and copy number variations in the VPS13A gene in patients with chorea-acanthocytosis. Am J Med Genet B Neuropsychiatr Genet 2011;156B:620–631.
40. Balikova I, Lehesjoki AE, de Ravel TJ, et al. Deletions in the VPS13B (COH1) gene as a cause of Cohen syndrome. Hum Mutat 2009;30:E845–E854.
41. Megarbane A, Slim R, Nurnberg G, et al. A novel VPS13B mutation in two brothers with Cohen syndrome, cutis verticis gyrata and sensorineural deafness. Eur J Hum Genet 2009;17:1076–1079.
42. Exome Aggregation Consortium. ExAC browser. Updated January 16, 2015. accessed December 2017 Available at: http://exac.broadinstitute.org.
43. Chun BY, Rizzo JF III. Dominant optic atrophy: updates on the pathophysiology and clinical manifestations of the optic atrophy 1 mutation. Curr Opin Ophthalmol 2016;27:475–480.
44. Jasoliya MJ, McMackin MZ, Henderson CK, et al. Frataxin deficiency impairs mitochondrial biogenesis in cells, mice and humans. Hum Mol Genet 2017;26:2627–2633.
45. Pierson TM, Adams D, Bonn F, et al. Whole-exome sequencing identifies homozygous AFG3L2 mutations in a spastic ataxia-neuropathy syndrome linked to mitochondrial m-AAA proteases. PLoS Genet 2011;7:e1002325.
46. Finsterer J. Ataxias with autosomal, X-chromosomal or maternal inheritance. Can J Neurol Sci 2009;36:409–428.
47. Shanmughapriya S, Rajan S, Hoffman NE, et al. SPG7 is an essential and conserved component of the mitochondrial permeability transition pore. Mol Cell 2015;60:47–62.
48. Bargiela D, Shanmugarajah P, Lo C, et al. Mitochondrial pathology in progressive cerebellar ataxia. Cerebellum Ataxias 2015;2:16.
49. Hayashi G, Cortopassi G. Oxidative stress in inherited mitochondrial diseases. Free Radic Biol Med 2015;88(pt A):10–17.
50. Anding AL, Wang C, Chang TK, et al. Vps13D Encodes a Ubiquitin-Binding Protein that Is Required for the Regulation of Mitochondrial Size and Clearance. Curr Biol 2018;28:287–295.e6.
51. Kim M, Sandford E, Gatica D, et al. Mutation in ATG5 reduces autophagy and leads to ataxia with developmental delay. Elife 2016;5.